the FEBS Journal

From steady-state to synchronized yeast glycolytic oscillations II: model validation

Franco B. du Preez[1,2], David D. van Niekerk[1] and Jacky L. Snoep[1,2,3]

1 Triple J Group for Molecular Cell Physiology, Department of Biochemistry, Stellenbosch University, Matieland, South Africa
2 Manchester Institute of Biotechnology, The University of Manchester, UK
3 Molecular Cell Physiology, Vrije Universiteit, Amsterdam, The Netherlands

Keywords
glycolysis; limit-cycle oscillation; mathematical model; model validation; *Saccharomyces cerevisiae*

Correspondence
J. L. Snoep, 1 Triple J Group for Molecular Cell Physiology, Department of Biochemistry, Stellenbosch University, Private Bag X1, Matieland 7602, South Africa
Fax: +27 218085863
Tel: +27 218085844
E-mail: jls@sun.ac.za

(Received 19 January 2012, revised 13 April 2012, accepted 1 June 2012)

doi:10.1111/j.1742-4658.2012.08658.x

In an accompanying paper [du Preez *et al.*, (2012) *FEBS J* doi: 10.1111/j.1742-4658.2012.08665.x], we adapt an existing kinetic model for steady-state yeast glycolysis to simulate limit-cycle oscillations. Here we validate the model by testing its capacity to simulate a wide range of experiments on dynamics of yeast glycolysis. In addition to its description of the oscillations of glycolytic intermediates in intact cells and the rapid synchronization observed when mixing out-of-phase oscillatory cell populations (see accompanying paper), the model was able to predict the Hopf bifurcation diagram with glucose as the bifurcation parameter (and one of the bifurcation points with cyanide as the bifurcation parameter), the glucose- and acetaldehyde-driven forced oscillations, glucose and acetaldehyde quenching, and cell-free extract oscillations (including complex oscillations and mixed-mode oscillations). Thus, the model was compliant, at least qualitatively, with the majority of available experimental data for glycolytic oscillations in yeast. To our knowledge, this is the first time that a model for yeast glycolysis has been tested against such a wide variety of independent data sets.

Database
The mathematical models described here have been submitted to the JWS Online Cellular Systems Modelling Database and can be accessed at http://jjj.biochem.sun.ac.za/database/dupreez/index.html.

Introduction

The traditional approach to model validation has been to compare model predictions with data sets that were not used for model construction. One could argue that it is misleading to use the term validation or verification for such a process; a high degree of truth/correctness is usually associated with a model that is validated and this cannot be based on comparison only. As our models are hypotheses for processes in the natural world, and are not formally closed systems, they can never be proven to be true, only disproven [1]. Much of the lack of clarity related to model validation appears to be due to the different meanings that are given to the process [2]. Formal approaches to model comparison and its application for model testing and rejection have recently been proposed for systems biology studies (e.g. [3]).

In systems biology studies, the aim is to quantitatively understand the systemic behavior on the basis of characteristics of the system's components and the interactions between them. Mathematical models are

Abbreviations
CSTR, continuous stirred-tank reactor; F16P, fructose-1,6-bisphosphate; G6P, glucose 6-phosphate; GAPDH, D-glyceraldehyde-3-phosphate dehydrogenase; PFK, 6-phosphofructokinase.

used to integrate the dynamics of the components' interactions, for instance enzyme activities in metabolic pathways. For model construction, kinetic data for isolated enzymes may be used to fit rate equations for each of the individual processes. The rate equations should be chosen to provide a good reflection of the kinetic data, with all parameters identifiable in the data set. *In vitro* kinetics have the advantage that sufficient perturbations can be made to estimate all parameter values even for detailed kinetic mechanisms, but care should be taken that the *in vitro* conditions reflect the *in vivo* conditions as much as possible.

The original Teusink model [4] for yeast glycolysis was constructed in this way, which is the main reason that we used this model for re-calibration [5]. The original validation of the Teusink model was for a single steady state, and the authors addressed the question whether *in vitro* kinetics can be used to predict an *in vivo* steady state. The model was able to correctly predict the *in vivo* flux through the glycolytic pathway (5% error in the ethanol production rate and 19% error in the glucose consumption rate), but there were considerable errors in prediction of some of the steady-state metabolite concentrations. Allowing for substantial changes of the parameter values, the steady state was described precisely. The strength of the Teusink model lies in the detailed kinetic mechanisms with an experimentally determined parameter set, and its ability to predict systemic behavior without fitting of parameter values to the data set. Importantly the validation data set was completely independent from the model construction data set.

A different approach for model construction (see [6] for a historical perspective on the two approaches), usually referred to as top-down modeling, is to fit model parameters to systems behavior. As the data sets for such systemic behavior are much smaller (because it is difficult to make independent intracellular perturbations), this leads to under-determined models or necessitates use of simple equations that not necessarily capture the components' characteristics sufficiently well. An additional problem with this approach is that it is hard to validate the model; the data sets for model construction and validation are often very similar in top-down approaches, and it is unclear what is tested in the model if these data sets are not independent. Important aspects of this top-down approach, such as experimental design, identifiability and estimation of parameters have been nicely summarized in a series of mini-reviews [7–9].

In an accompanying paper, we re-calibrate the Teusink model to describe limit-cycle oscillations [5]. The necessity for re-calibration was due to the different experimental conditions used for the study of glycolytic oscillations compared to the conditions used for the Teusink study [4]; i.e. different yeast strain and incubation conditions (glucose starvation). Using a limited data set, it was possible to adapt the Teusink model by three optimization steps to describe rapid in-phase synchronization of yeast glycolytic oscillators. In addition to changes in expression levels of the enzymes, only seven parameters required alteration by more than 20%, and five of these parameters were associated with the phosphofructokinase reaction.

Although adaptations to the original model were small, and mostly fall within the experimental error of the parameter determinations, the real value of the model lies in its ability to describe and predict experimental data that were not used for its calibration. In this paper, we test this newly constructed model for its ability to simulate a wide set of experiments on oscillations of yeast glycolysis in whole cells and cell-free extracts. This test does not constitute a model validation in the sense that all aspects and parameters of the model are verified, but rather tests the compliance of the model with a wide range of experimental data that were not used for model calibration. For the model predictions, we did not make changes in the intracellular model parameters and we tried to match the external conditions as closely as possible to the experimental set-up. However, in some of the validation experiments where we could not reproduce the experimental results qualitatively, we have allowed for small changes in simulations of the experimental set-up. We restrict the model validation to the ability of the model to simulate the available experimental data for yeast glycolytic oscillations, and to provide insight into the molecular mechanism underlying the system behavior. In a third paper [10], we use the model to identify experimental conditions under which isolated yeast cells display limit-cycle oscillations.

Results

In an accompanying paper [5], we adapt a steady-state model for yeast glycolysis [4] to simulate limit-cycle oscillations. An important test for the model is its predictive capacity for experimental data that were not used for fitting in the optimization steps. We started with model validation by comparing model simulations with experimental data for the limit-cycle oscillations [5]. This represents validation of the model for the time-dependent behavior of the glycolytic intermediates, i.e. prediction of amplitude and phases of intermediates. For the final model, very similar simulation results were obtained for the metabolite amplitudes

and phases compared to the experimental values [5]. There are clear limits to the accuracy of amplitudes and phases that can be extracted from the experimental data [11] due to inter-cycle variations and experimental error, but the model prediction overlaps most of the experimentally measured values in terms of the range of concentrations for each metabolite, and individual oscillations for the model and data are mostly aligned throughout one period. A second validation of the model involved description of the mixing of two out-of-phase yeast cultures as described previously [12,13]. The experimental data for this experiment were not used in the optimization for synchronization, although one could argue that the data are implicit in formulation of the optimization criterion for maximal synchronization.

In addition to these first model validations, we subsequently searched the scientific literature for additional experimental data for oscillatory yeast cultures to test our model.

Bifurcation diagram for glucose

A rich experimental data set for oscillatory yeast cultures has been accumulated in the Sørensen lab [14,15,22,24,25]. They incubated yeast cells in a continuous stirred tank reactor (CSTR) set-up for experimental determination of bifurcation diagrams for glucose and cyanide concentrations in the feed medium. We transferred our model to a CSTR set-up (in the dupreez5 model), i.e. inclusion of glucose and cyanide inflow reactions and outflow reactions for all external metabolites (biomass is modeled as if it is retained in the reactor [14]) (see Fig. 1 for the reaction network). None of the parameters in the dupreez4 [5] model were changed in the dupreez5 model.

We simulated the CSTR set-up using the dupreez5 model at various glucose concentrations in the feed. The simulation results for NADH are shown in Fig. 2. It should be noted that the NADH fluorescence measured in the experiments was not converted to internal concentrations by the researchers and was published in arbitrary units [14]. The fluorescence signal was normalized to the maximal amplitude of the model simulations. As such, the amplitude in Fig. 2 is not a validation of the model, but the positioning of the Hopf bifurcation point and the 'opening up' of the diagram, i.e. the range of glucose concentrations over which the amplitude increases to its maximal value, are independent model validations. The supercritical Hopf bifurcation point in the model (19.3 mM glucose in the feed) is remarkably close to the experimentally measured value (18.5 mM). In addition, the increase in amplitude with increasing glucose concentrations in the feed is very similar to the experimentally observed dependency: for the experimental data, 90% of the maximum amplitude is reached at a glucose concentration that is 7 mM higher than the bifurcation point [14], while for the model it is reached at a concentration that is 5.7 mM higher). Although the bifurcation points for the glucose concentration in the feed are very similar for the model and the experimental data, the glucose concentration in the reactor is somewhat higher in the model.

Cyanide bifurcation

In addition to glucose, cyanide can also be used as a bifurcation parameter. Two bifurcation points were observed experimentally [14] (Fig. 3), and population oscillations exist only between the two points. In the experiments, 28 mM of glucose was used in the feed medium. The combination of this high glucose concentration and the CSTR set-up resulted in synchronized oscillations in the absence of cyanide in our model simulations. To observe the supercritical Hopf bifurcation point at the experimentally observed cyanide concentration (4 mM), we lowered the glucose concentration in the feed from 28 to 20 mM. Our model does not show the second bifurcation point at high cyanide concentrations that was observed experimentally. The simulation results show a maximum amplitude at 11.5 mM of cyanide, but upon increasing the cyanide concentration above 16 mM, the model simulations show similarities to the *tps1*Δ mutant phenotype [16], characterized by accumulation of hexose phosphates in the upper part of glycolysis. This model behavior excludes limit-cycle oscillations, and thus we were not able to further analyze the bifurcation diagram at higher cyanide concentrations.

Mean glucose consumption rates

During the optimization procedures for re-calibration [5], we adjusted the V_{max} values of all reaction steps to set the frequency of the oscillations to the experimentally observed values. If all reaction steps are perturbed equally, the time unit in the system and thus the frequency of the oscillations are re-scaled. This is very clear in metabolic control analysis summation theorems; all observables with time units have summations theorems equalling 1 (e.g. the Reijenga frequency summation theorem [17]). Thus, it is possible to set the frequency without perturbing many of the other characteristics, such as metabolite profiles, bifurcation points, amplitudes etc.

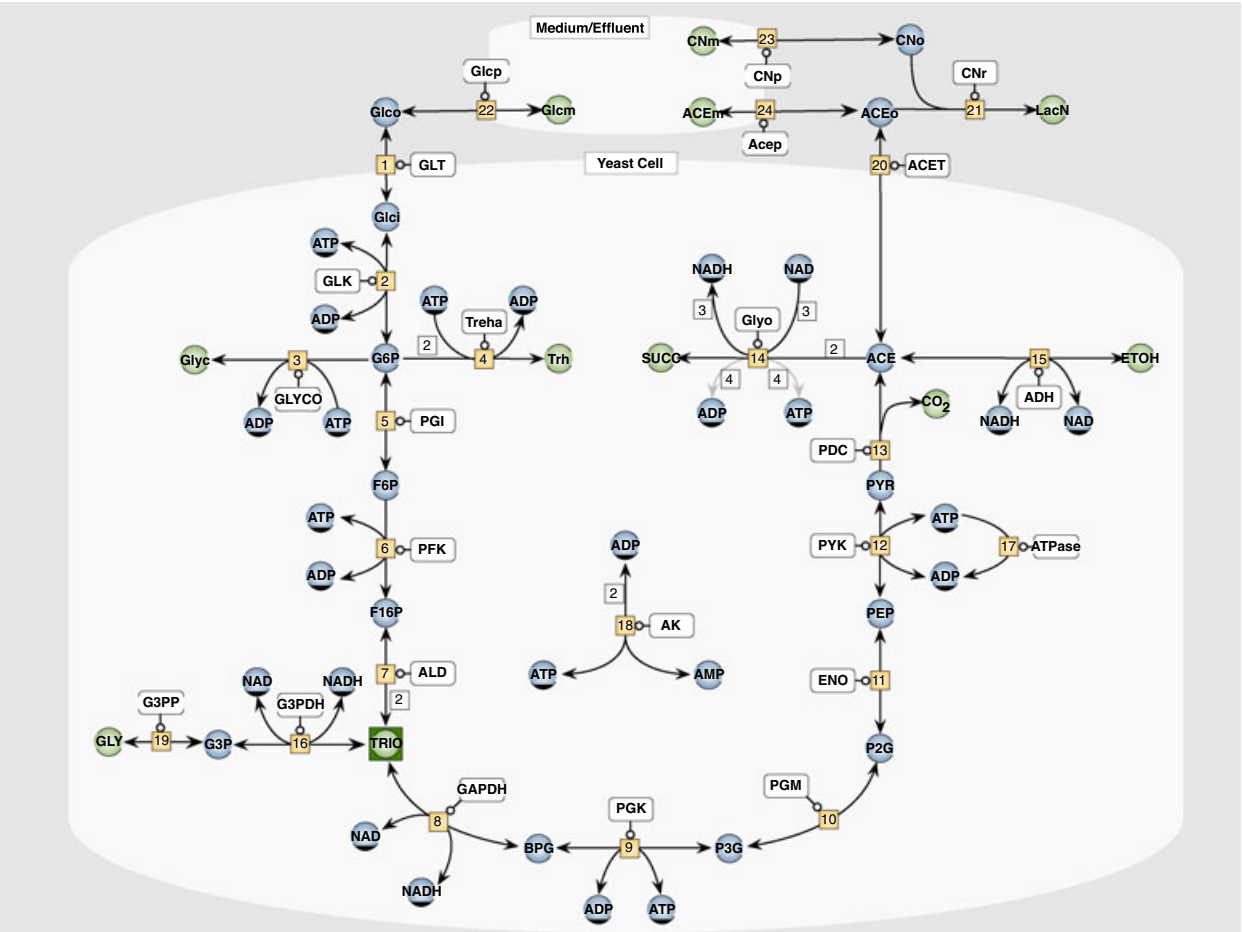

Fig. 1. Reaction network for the glycolytic models. The original Teusink model consists of reactions 1–18, constituting glucose transport, glycolysis, and the branch reactions to trehalose, glycogen and succinate. In the Teusink model, reactions 16 and 19 were combined as a single reaction for glycerol production, and reaction 18 was modeled as an equilibrium block. The reaction network for the dupreez4 model consists of reactions 1–21, whereby reactions 20 and 21, acetaldehyde transport and complex formation with cyanide, were added to include cell–cell interactions, which is necessary for the synchronization studies [5]. For the CSTR set-up as modeled in dupreez5, we added (pump) reactions 22–24 to the reaction network in dupreez4. For cell-free extract simulations in a closed system (dupreez6), the reaction network consists of reactions 2–19 and 22; cell-free extract simulations in a CSTR (continuous stirred-tank reactor) (dupreez7) consist of reactions 2–19 and additional inflow and outflow reactions for all metabolites. ACE, acetaldehyde; ADH, alcohol dehydrogenase (EC 1.1.1.1); AK, adenylate kinase (EC 2.7.4.3); ALD, fructose-1,6-bisphosphate aldolase (EC 4.1.2.13); BPG, 1,3-bis-phosphoglycerate; ENO, phosphopyruvate hydratase (EC 4.2.1.11); F16P, fructose-1,6-bisphosphate; F6P, fructose 6-phosphate; GAP, D-glyceraldehyde-3-phosphate; GAPDH, D-glyceraldehyde-3-phosphate dehydrogenase (phosphorylating) (EC 1.2.1.12); G3P, glycerol 3-phosphate; G3PDH, glycerol 3-phosphate dehydrogenase (EC 1.1.99.5); G6P, glucose 6-phosphate; GLYCO, glycogen branch; HK, hexokinase (EC 2.7.1.1); P2G, 2-phosphoglycerate; P3G, 3-phosphoglycerate; PEP, phosphoenolpyruvate; PDC, pyruvate decarboxylase (EC 4.1.1.1); PGI, glucose-6-phosphate isomerase (EC 5.3.1.9); PFK, 6-phosphofructokinase (EC 2.7.1.11); PGK, phosphoglycerate kinase (EC 2.7.2.3); PGM, phosphoglycerate mutase (EC 5.4.2.1); PYK, pyruvate kinase (EC 2.7.1.40); PYR, pyruvate; TPI, triose phosphate isomerase (EC 5.3.1.1); Tps1, trehalose 6-phosphate synthase (EC 2.4.1.15); TREHA, trehalose branch; SUC, succinate branch.

However, other characteristics with time units will also scale, and thus it is important to check that these characteristics show the correct behavior after adjusting the V_{max} values during the optimization procedures. The most obvious characteristic to check is the flux through the system, e.g. glucose conversion to ethanol. Experimentally, the oscillatory flux is hard to measure, but a mean flux of 54.19 mmol glucose·L^{-1} cytosol·min^{-1} has been determined during glycolytic oscillations [18]. This is a much lower flux than observed in the validation experiments for the original Teusink model, i.e. 108 mmol glucose·L^{-1} cytosol·min^{-1}, with a corresponding steady-state flux value of 88 mmol glucose·L^{-1} cytosol·min^{-1} in the Teusink model. It is known that the

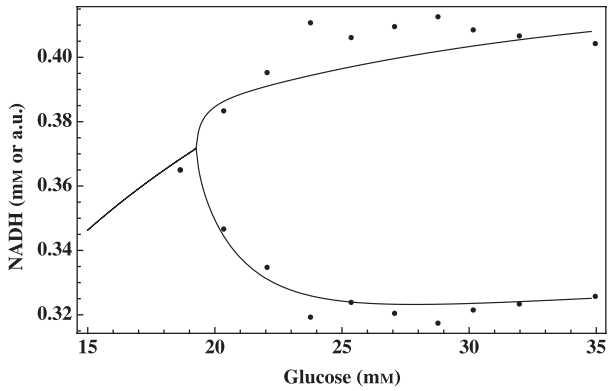

Fig. 2. Hopf bifurcation for glucose in CSTR experiments and model prediction. The glucose concentration in the feed was varied and the effect on NADH fluorescence of a cell population was monitored. Experimental data (closed circles; arbitrary units, AU) are from Hynne *et al.* [14]; model simulation (solid line; mM) is by dupreez5.

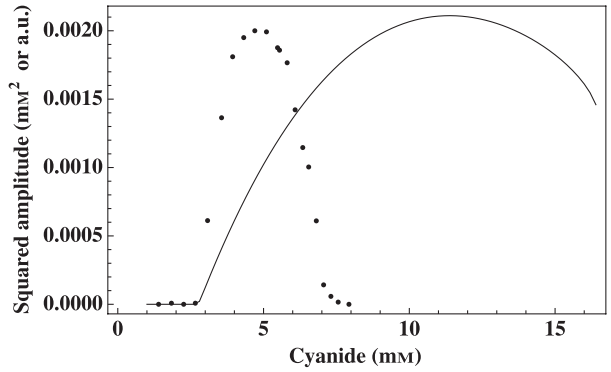

Fig. 3. Hopf bifurcation for cyanide in CSTR experiments and model prediction. The cyanide concentration in the feed was varied and the effect on NADH fluorescence was monitored. Experimental data (closed circles; arbitrary units, AU) are from Hynne *et al.* [14], model simulation (solid line, mM) is by dupreez5. The experimental data were captured from two experiments, one with 28 mM glucose in the feed and the other with 27 mM glucose. For the model simulation, we used a 20 mM glucose concentration in the feed.

glycolytic capacity of yeast decreases during starvation [19,20], and as this is part of the preparation of the cells before oscillation experiments, this may have led to the observed decrease in flux in these experiments. During our optimization procedures (5), and in setting the frequency, V_{max} values of enzymes were decreased, and it was important to check that our predicted flux was still comparable to the experimentally measured flux values. The dupreez4 model has a mean flux of 44.78 mmol glucose·L^{-1} cytosol·min^{-1}, which compares well with the measured flux value of 54.19 mmol glucose·L^{-1} cytosol·min^{-1}.

For a CSTR set-up as described previously [14], we calculated the mean fluxes over the main glycolytic pathway and its branches at 20 mM extracellular glucose concentration for both the Hynne model [14] and our dupreez5 model. The values for both models are in reasonable agreement, although the Hynne model has consistently higher fluxes through the pathways branching from glycolysis, i.e. 49.04 and 40.77 mM·min^{-1} for the mean glucose consumption rate flux, 20.39 and 8.32 mM·min^{-1} for the flux to storage carbohydrates, 5.16 and 1.73 mM·min^{-1} for the flux to glycerol, and 46.97 and 56.46 mM·min^{-1} for the ethanol production flux, for the Hynne and dupreez5 models, respectively.

Cell-free extract oscillations

The available kinetic models for yeast glycolysis simulate either intact cells or cell-free extracts. As the vast majority of the enzymes in the two systems are identical, it should be possible to simulate both types of oscillations with the same model, with minimal adjustments with respect to protein concentration and transport reactions. Interestingly, the absence of transport reactions is expected to lead to differences between the two systems; in particular, the glucose and acetaldehyde transport steps have a large effect on the oscillatory behavior in whole-cell incubations.

To simulate cell-free extract oscillations [21], we simply omitted the transport steps in the dupreez4 model, diluted the enzyme activity according to the concentration measured [21], reduced the co-factor concentrations to those reported, and ran time simulations. At the glucose inflow rate of 0.83 mM·min^{-1} reported, the internal glucose concentration was too low to observe oscillations. With this given input flux, oscillations were observed only for a narrow range of biomass concentrations, which were quite far removed from the experimental value (22% of original value). In addition, we altered the ATPase kinetics (V_{max} 110% and K_M 20% of the value in dupreez4) to obtain simulations that were similar to the experimental data (Figs 4 and 5). The period of the oscillations in the simulation (8.8 min) was close to the experimentally observed period ($\sim$ 10 min). Note that under these conditions (fixed influx rate), the period of the oscillations does not scale with the protein concentration.

We also compared our model to another cell-free extract study [22] that was performed at a protein concentration of 5 mg·mL^{-1} in a CSTR set-up. We

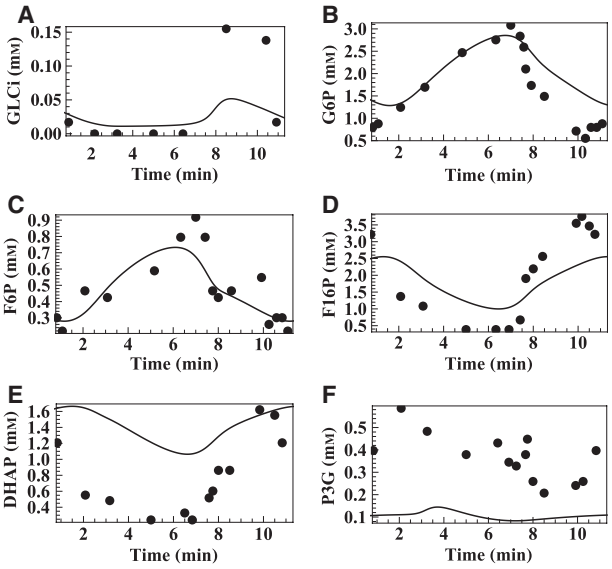

Fig. 4. Comparison of model simulations (dupreez6, solid line) to experimental data [21] for glycolytic intermediate (see Fig. 1) concentrations in cell-free extracts.

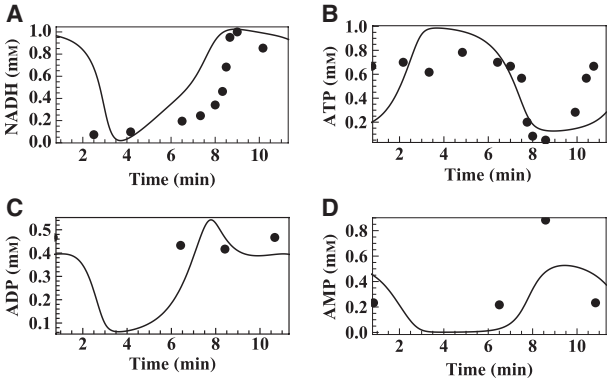

Fig. 5. Comparison of model simulations (dupreez6, solid line) to experimental data [21] for co-factor concentrations in cell free extracts.

simulated these experiments (model dupreez7, see below for details), and obtained comparable results with a 1.4-fold higher protein concentration. The authors reported an oscillatory period of 14 min [22], whereas we obtained a period of 16 min. A more detailed comparison between our CSTR extract model and the study described previously [22] is given below.

Complex oscillations in cell-free extracts

Chaotic and complex periodic behavior of glycolytic intermediates in yeast extracts has been observed in a CSTR set-up [22]. Simple oscillations, complex periodic oscillations or chaos were observed experimentally and in a mathematical model as a function of the glucose influx rate.

We simulated these experiments by adjusting the dupreez6 model to the CSTR set-up, leading to dupreez7. In the experiment, extract (consisting of enzymes and unknown concentrations of metabolites), glucose, NADH and ATP are pumped into the reaction chamber. The reaction chamber has a constant volume, and the extract and all metabolites are removed from the chamber at a rate equal to the influx rate. For model adjustment, we added reactions for influx and efflux of all metabolites, and we chose intermediate concentrations in the inflowing medium. These intermediate concentrations were chosen to be close to the steady-state intermediate concentrations at 50 mM glucose, i.e. ATP, 1.25; AMP, 0.0399; ADP, 0.279; NAD, 0.798; NADH, 0.199; glucose, 52.2; bisphosphoglycerate, 0.0000673; fructose-1,6-bisphosphate (F16P), 7.85; fructose-6-phosphate (F6P), 0.448; glycerol 3-phosphate (G3P), 0.884; glucose 6-phosphate (G6P), 2.18; 2-phosphoglycerate (P2G), 0.0131; 3-phosphoglycerate (P3G), 0.126; phosphoenolpyruvate (PEP), 0.00982; pyruvate (PYR), 1.88; sum of triose phosphates (TRIO), 2.99; acetaldehyde (ACE), 0.0204 (values in mM). The protein concentration in the experiments was 5 $mg \cdot mL^{-1}$. To simulate this, we adjusted the V_{max} values in the model (which are based on 267 $mg \cdot protein \cdot mL^{-1}$ cytosol) by a factor of 5/267. To be able to reproduce the dynamic behavior, we required an additional 1.43 dilution factor for the protein concentration. The only enzyme kinetic parameters that were changed in the model were for the ATPase reaction: we adjusted the K_M value for ATP to 0.188 mM and lowered the V_{max} value to 0.0164 $mM \cdot min^{-1}$.

In Fig. 6, we show the various types of dynamic behavior observed in the CSTR cell-free extract experiments [22], together with the model simulations (dupreez7). The experimental data and model simulations display steady state, harmonic, relaxation and complex oscillations as a function of the flow rate. The flow rate is the only parameter that was varied for the experiments and simulations shown in Fig. 6A–J, with dilution rates (min^{-1}) of 0.0244, 0.0247, 0.026, 0.03, 0.025 and 0.0253 for Fig. 6A,C,E,G,I, and 0.012, 0.015, 0.024, 0.03, 0.019 and 0.021 for Fig. 6B,D,F,H,J. Although the various types of behavior were reproduced in the model simulations, there are some quantitative differences between model simulations and experimental data, notably in dilution rates and frequency, and also in the shape of the relaxation oscillations.

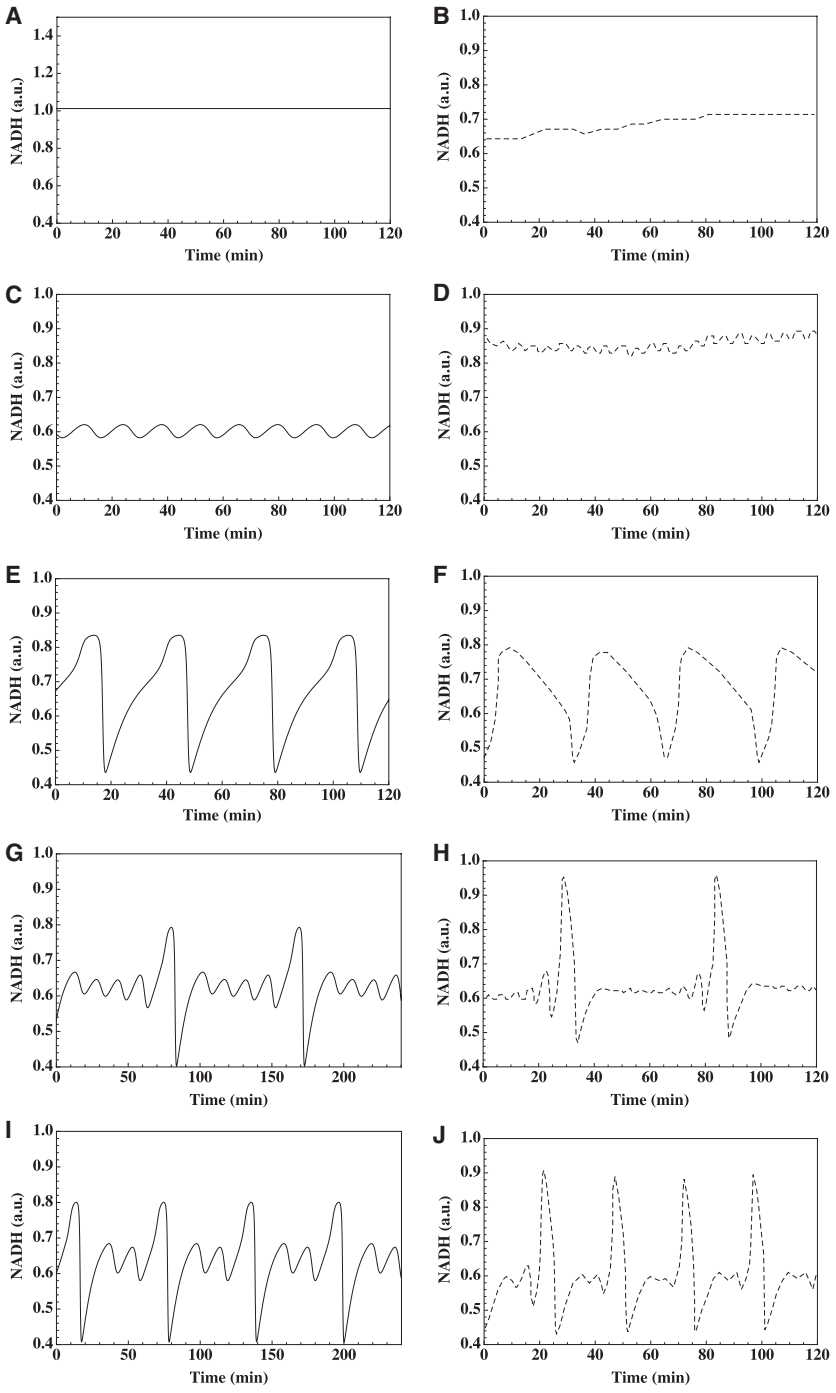

Fig. 6. Comparison of model simulations to experimental data [22] for complex dynamics in cell-free extracts. Model simulations (dupreez7) for NADH dynamics are shown on the left and corresponding experimental data [22] on the right. At different influx rates of glucose, different behavior is observed: (A,B) steady state; (C,D) harmonic oscillations; (E,F) relaxation oscillations; (G–J) complex oscillations (mixed-mode oscillations).

ATP–NADH phase-plane plots

A phase-plane plot analysis of variables during a limit-cycle oscillation provides detailed information on the phase difference and the shape of the oscillations of the variables. The phase difference can be calculated from a phase-plane plot for harmonic waves, and a comparison between the model and the experiments can be made. The shape of the phase-plane plot gives information on the distance from the Hopf bifurcation under which the experiment (or simulation) was performed. The further away from the Hopf bifurcation, the stronger the deviation from ellipse-shaped curves.

Few experimental studies have been published in which the authors sampled the oscillations frequently enough to construct phase-plane plots. For whole-cell

studies, the Richard data set [11] is not accurate enough for such an analysis; three periods are shown in the paper and these have quite a large variability. However, in a more recent paper [23], ATP was measured online using aptamer-based biosensors, while simultaneously following NADH fluorescence. For these experiments, an ATP–NADH phase-plane plot could be constructed. In addition, we were able to use the data set of Das and Busse [21] for cell-free extracts, which had good resolution for NADH and ATP oscillations. We compare both phase-plane plots with model simulations (dupreez4) in Fig. 7. It is difficult to obtain absolute values for the NADH fluorescence signal in the experimental data sets, and these are usually reported as arbitrary units. For ATP concentrations, very different mean values and amplitudes have been reported: Richard *et al*. report an amplitude of 0.6 mM and a mean concentration of 2.1 mM [11], Ozalp *et al*. [23] reported a much smaller amplitude with a mean concentration, and Das and Busse [21] measured a much lower mean concentration with a relatively large amplitude in cell-free extracts.

The phase difference between the peak values of NADH and ATP was similar in the experimental data set of Ozalp *et al*. [23] and our model simulations, i.e. close to 150°, but the ATP phase is reported as 180° by Richard *et al*. [11]. In comparison, the Hynne model [14] predicts a similar phase difference of 139°. For the extract data of Das and Busse [21], the authors fitted a line rather than an ellipse (Fig. 7B), indicating a 180° phase difference. The shape for the phase-plane plot in Ozalp *et al*. [23] indicates that these experiments were performed closer to the Hopf bifurcation, while the Das and Busse experiments [21] and the dupreez4 model showed very similarly shaped phase-plane plots.

Quenching of the oscillations

Quenching of the yeast glycolytic oscillations by addition of the extracellular metabolites glucose and acetaldehyde has been described previously [15]. Addition of either of these extracellular metabolites brings their concentrations close to their unstable steady state values, and this leads to temporary silencing of the oscillations. As such, quenching is strongly dependent on the concentration of the metabolite that is added and its phase in the oscillatory system.

In Fig. 8, we show a comparison for experimental [15] and simulated (dupreez5) quenching by acetaldehyde or glucose addition. Experimentally, 98 μM acetaldehyde added at a phase of 172° resulted in

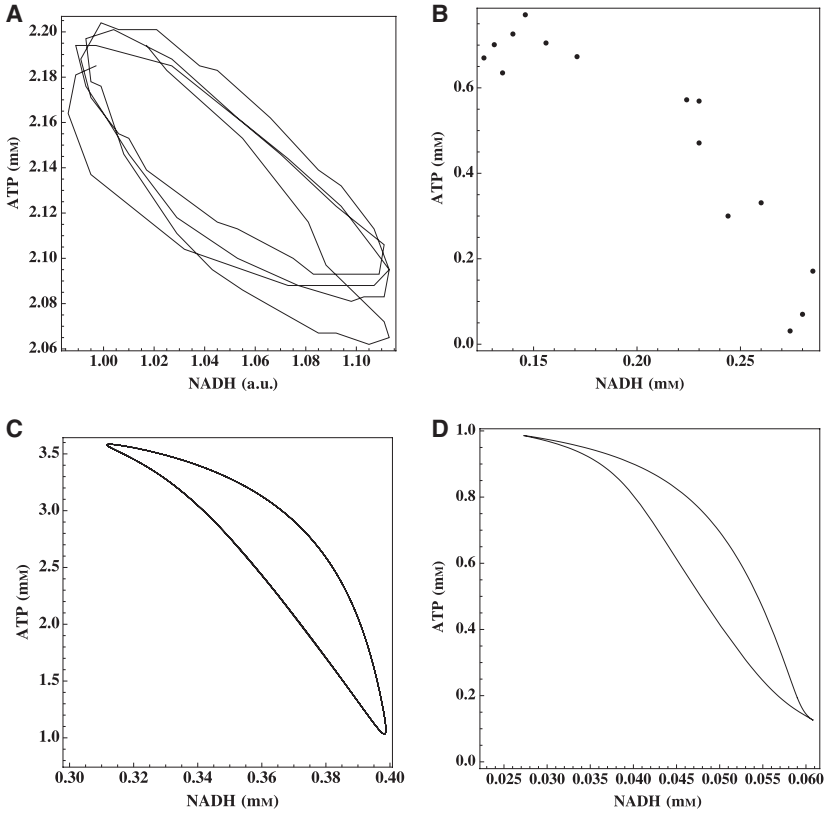

Fig. 7. Comparison of NADH–ATP phase-plane plots. (A) Experimental data for whole cells [23], (B) experimental data for cell-free extracts [21], (C) model simulation for whole cells (dupreez4) and (D) model simulation for cell-free extracts (dupreez6).

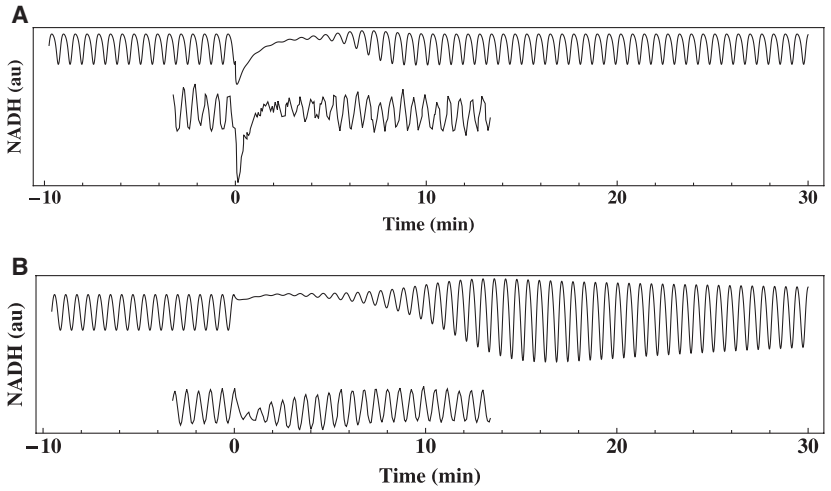

Fig. 8. Quenching of the oscillations. (A) Acetaldehyde quenching; (B) glucose quenching. Simulations using dupreez5 are shown at the top of (A) and (B), and experimental data [15] are shown at the bottom.

quenching. For the model, we required addition of 7.2 μM acetaldehyde at 224°. Thus, although the phase of addition in the model simulation is similar to the experimental phase, the concentration of acetaldehyde is much lower in the model than in the experiment. As shown in Fig. 8A, the simulated and experimental traces show similar effects upon acetaldehyde addition at $t = 0$, but more precise quenching was achieved in the simulation. Note that both the time point of addition (phase of oscillation) and the concentration of quenching metabolite are important, and this is hard to control precisely under experimental conditions.

For glucose, quenching was obtained experimentally by adding 1.11 mM at 4° (15). For the model, we obtained maximal quenching by addition of 0.86 mM glucose at 19.5°. The phase of the oscillation and the concentration of quenching metabolite are very similar for the model and the experiment. As observed for acetaldehyde quenching, glucose quenching was more complete in the model simulations than in the experiment.

Frequency dependence on external glucose

The oscillation frequency is known to be dependent on the external glucose concentration. Increasing the glucose concentration results in a small increase in oscillation frequency (0.086 rad*min^{-1}·mM^{-1} glucose in the CSTR medium, [14]). We checked the frequency response to glucose in our model, and observed that the frequency of the oscillations decreased with increasing glucose concentrations (−0.07 rad*min^{-1}·mM^{-1} extracellular glucose). In Fig. 9, we compare the frequency dependency on external glucose concentration for the experimental data set [14] with the model simulations.

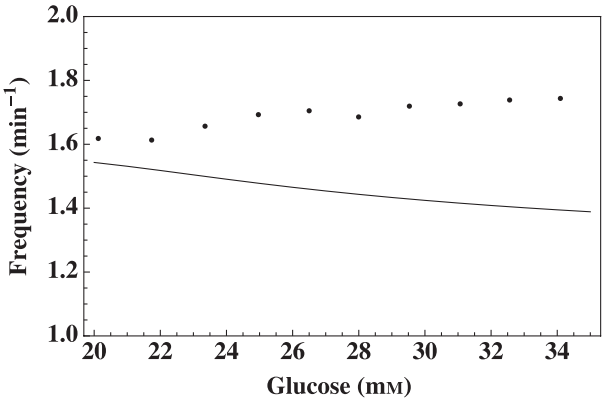

Fig. 9. Frequency dependency for glucose. Frequency of the glycolytic oscillations in intact cells as a function of the glucose concentration for experimental data [14] (closed symbols) and model simulations (dupreez5, solid line).

Although there is only a relatively low sensitivity for the external glucose concentration, the model prediction is qualitatively wrong. Reijenga *et al.* determined the control of the glucose transporter on the oscillatory frequency, and also noted a positive control [18]. Thus both types of experiments indicate a positive effect of glucose on the oscillatory frequency while our model shows a negative effect on the frequency. The Hynne model [14] also shows a negative correlation between glucose concentration and frequency.

Frequency and amplitude dependence on biomass concentration

De Monte *et al.* [24] determined the frequency and amplitude dependency on biomass concentration for yeast glycolytic oscillations in intact cells. The experimental set-up was similar to that used in the CSTR

experiments, with a dilution rate of 0.062 h^{-1} and saturating glucose concentrations (60 mM). Both the amplitude and frequency of the oscillations increased with biomass (Fig. 10). We simulated the experiments using the dupreez5 model, with a similar dilution rate (0.05 h^{-1}) but with a higher glucose concentration to ensure saturation at higher biomass values (300 mM). The model shows qualitative agreement with the experimental data; both the amplitude and frequency of oscillation increased with increasing biomass. However, at low biomass concentrations, the model displayed the *tps1*Δ phenotype [16], with accumulation of glucose 6-phosphate, fructose 6-phosphate and fructose 1,6-bisphosphate, preventing comparison between the model simulations and the experimental data at biomass concentrations below 5 mg·mL^{-1}.

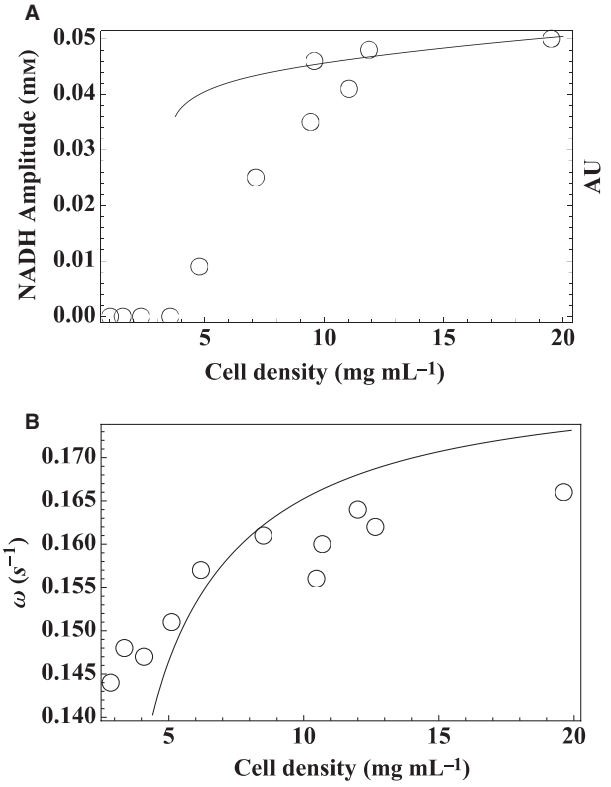

Fig. 10. Amplitude and frequency dependency for biomass concentration as determined previously [24]. Open circles indicate experimental values and solid lines represent model values (dupreez5). Note that model simulations show *tps1*Δ phenotype at biomass concentrations below 5 mg·mL^{-1}, and simulation results are therefore only given for higher concentrations. The biomass concentration (in g dry weight/ml) for the dupreez5 model was determined assuming a cytoplasmic protein concentration of 0.267 g protein·mL^{-1} [4] and 2 mg dry weight per mg protein. The NADH amplitude is measured experimentally in arbitrary units (AU) and can only be compared in relative terms to the mM units in the model simulations.

Forced oscillations

Synchronization between yeast cells has been studied via phase shifts in forced oscillatory experiments [25]. In an open flow reactor, yeast populations are entrained with either glucose or acetaldehyde at their natural frequency, and then subjected to a 180° phase shift. The phase shift in the entrainment signal led to a gradual decrease in the oscillation amplitude of the yeast population and a subsequent recovery to its original amplitude. We simulated the phase-shift experiments using our model (dupreez5), and obtained results that were qualitatively comparable to those obtained in the experiments when allowing reasonable variations in the experimental parameters for the simulations. Thus, we were able to entrain the yeast population with a driving oscillation at its natural frequency, and caused a temporary decrease in amplitude by 180° phase shifts in either glucose or acetaldehyde (Fig. 11).

For glucose forcing, we used a mean medium concentration of 19.3 mM glucose (21 mM in the experiment), which results in an extracellular concentration of 5.2 mM glucose (4.5 mM in the experiment). For acetaldehyde forcing, we used 23.5 mM glucose in the medium (60 mM in the experiment). No other parameters were modified for the simulations. As observed in the forcing experiments, we noticed a stronger reaction of the cell population to the acetaldehyde phase shifts than to the glucose phase shifts. In Fig. 11, the forcing amplitudes used were 79 and 130 μM for glucose, and 0.2 and 2 μM for acetaldehyde in the simulations and the experiments. As observed in the quenching experiments, the acetaldehyde concentrations for the model simulations were significantly lower than in the experiments.

Danø *et al.* [25] reported a decreasing minimum amplitude of the NADH oscillations and an increasing amplitude decay rate as a function of increasing resonant acetaldehyde forcing amplitude in 180° phase shift experiments. The dupreez5 model shows qualitatively similar behavior (data not shown), but, due to the large difference in external acetaldehyde concentrations in our model simulations compared to experimental values, we have not performed a quantitative analysis of these experiments.

Discussion

This is the second paper in a series of three, dealing with the construction [5], validation (this paper) and application [10] of a detailed glycolytic model of yeast glycolysis. Model construction mostly comprised

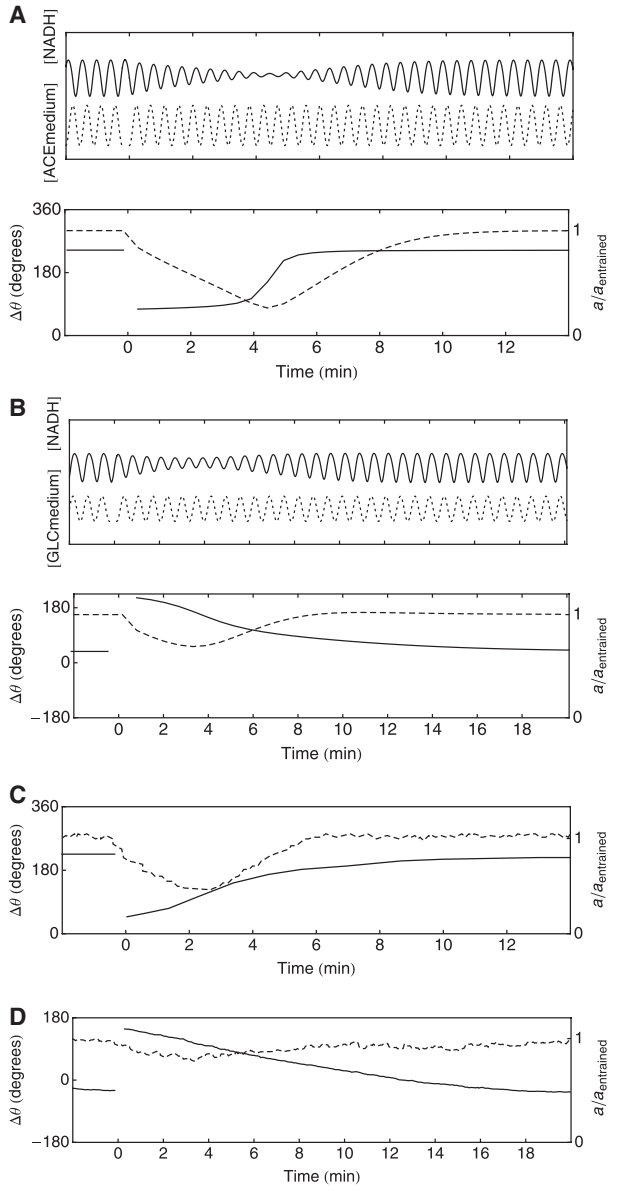

Fig. 11. Phase shifts in entrainment oscillations. (A) and (B) show the model simulations for the phase shift in the entrainment signal for acetaldehyde and glucose respectively. (C) and (D) show the experimental data for these studies. For the model simulation results, the *y* axis scales are in arbitrary units and are different for (A) and (B).

re-calibration of an existing model to adapt it to a different yeast strain and environmental conditions, in order to simulate glycolytic oscillations. In this paper, we focus on testing the model for its compliance with available experimental data, and in the third paper, we apply the model to explore new experimental conditions for studying oscillations in isolated yeast cells.

Although we used a number of models to simulate the various experiments, these models only differ in the extracellular environment, i.e. the yeast model itself was not changed (with the exception of the cell-free extract models, where the transporters were removed from the model). For the re-calibration, we used a small data set [5], and we were able to simulate a large number of experiments using the resulting model. The model correctly predicted the phases and amplitudes of most of the glycolytic intermediates, but only the amplitude for F16P was used for model calibration. The predictive power of the model for the Hopf bifurcation plot with the glucose concentration as bifurcation parameter was striking (Fig. 2), but the same plot as a function of the cyanide concentration was less precise (Fig. 3), i.e. the second bifurcation at high concentrations could not be simulated. Both the glucose and cyanide bifurcation plots were also simulated by the Hynne model [14]. It should be noted that the Hynne model was fitted to experimental data at the Hopf bifurcation point, thus the ability of the Hynne model to describe the bifurcation point is not a validation but its ability to describe behavior away from the bifurcation point is. The Hynne model describes the glucose bifurcation very similarly to our dupreez5 model. Interestingly, for the cyanide bifurcation, the Hynne model was only able to describe the Hopf bifurcation at the high cyanide concentration but not the bifurcation at the lower concentration. Thus neither the Hynne model nor the dupreez5 model were able to describe both Hopf bifurcation points in the cyanide bifurcation experiment.

The model was in qualitative agreement with the glucose and acetaldehyde quenching experiments (Fig. 8) and the forced oscillation experiments (Fig. 11). The Hynne model [14] was in better agreement with the glucose and acetaldehyde quenching experiments, but it should be noted that these experiments were used for model fitting, i.e. the model is tested whether it can describe the data, while, for our model, the simulations are model predictions of the experiments. Our model was able to simulate cell-free extract oscillations (Figs 4–6) by removing the transport steps and adjusting the protein concentration and ATPase kinetics. In some of the simulations, we were not able to directly simulate the experiments and had to make small changes to model parameters. In those cases, the simulation is not a direct prediction of the model but a test as to what extent the model parameters must be changed to simulate the experiment. For instance, in the cell-free extract simulations, we made significant changes to the protein concentrations compared to the experimental values.

In some of our validation simulations, e.g. in the cyanide bifurcation plot (Fig. 3), we observed that model simulations showed similarity to the *tps1*Δ mutant phenotype [16]. The phenotype of this deletion strain comprises accumulation of hexose phosphate intermediates and an inability to grow at high glucose concentrations. As trehalose-6-phosphate inhibits upper glycolysis at the level of glucose phosphorylation via hexokinase 2 [26], it normally prevents lethal build-up of phosphorylated intermediates. The Teusink model does not include detailed kinetics for the trehalose branch, and we did not include any regulatory loop via trehalose 6-phosphate. As such the model has no negative feedback to the hexokinase or glucose transporter, making it susceptible to the *tps1*Δ phenotype. Other kinetic models for yeast glycolysis [14,27] have incorporated feedback inhibition of G6P onto the glucose transporter, and this significantly increases the stability of the system. However, there is no biochemical evidence for such inhibition, and we hold to the premise of the Teusink model to only include existing biochemical knowledge, and therefore did not include G6P inhibition on glucose transport in the model.

In most of the validation simulations, we were able to reproduce the experimental data sets at least qualitatively and in some cases quantitatively. An exception where we obtained a qualitatively different result is for the glucose dependency of the frequency of the oscillations (Fig. 9). Whereas experimentally there is a small increase in frequency with increasing glucose concentrations, we observed a small decrease in frequency in our simulations. Although the effect of glucose on the observed frequency is small, it is qualitatively different from our model simulations. To our knowledge, there is currently no detailed kinetic model for yeast glycolysis available that describes the frequency response for glucose correctly, and an incorrect prediction is also made for the frequency dependence on glucose in the Hynne model [14]. However, in some core models, correct dependency has been obtained [28]. We were not able to change this frequency response on the basis of the given kinetic rate equations and structural network. When we made changes to the reaction stoichiometry in the storage carbohydrate branches, we were able to get a qualitatively correct frequency response, but many of the other oscillatory characteristics were changed. We decided to keep our kinetics for the carbohydrate branches simple until experimentally measured kinetic data become available. Both the *tps1*Δ phenotype and the wrong frequency response are related to the branches to glycogen/trehalose, providing motivation to obtain more detailed kinetics for these branches.

Our model validation criterion is linked to model function, whereby we focus on compliance with existing experimental data and helping to understand the regulatory mechanism of yeast glycolytic oscillations. For this second function, it is important to include known regulatory mechanisms only, and use experimentally measured parameter values as much as possible. In all the simulation experiments presented in this paper, we noticed an important role for the adenine nucleotide and the nicotinamide adenine nucleotide co-factors. An important role for these co-enzymes has been shown previously [29], whereby transduction of the oscillation from the lower part of glycolysis to the upper part could be established by the co-factors independent of the carbon intermediates. In the re-calibration [5], the various steps in the optimization indicate the various roles the co-enzymes play; the adenine co-enzymes are crucial to move the model into an oscillatory mode, which may be related to the levels of ATP that are inhibitory for 6-phosphofructokinase (PFK), while the nicotinamide adenine nucleotide co-factors are important for intercellular communication, i.e. synchronization via acetaldehyde.

In the re-calibration [5], we changed the steady-state model to an oscillatory model by perturbations to enzymes that have high control on the ATP concentration (ATPase and glucose transport), and by perturbing enzymes that increase the ATP sensitivity of the PFK via increases in the F16P concentration (e.g. D-glyceraldehyde-3-phosphate dehydrogenase, GAPDH). In another optimization step, focusing on strong synchronization, parameter adjustments mostly affected the $NADH/NAD^+$ ratio. Whereas the extracellular communication between the cells is via acetaldehyde, this is transferred via a fast transport step to intracellular acetaldehyde and via alcohol dehydrogenase to the $NADH/NAD^+$ couple. The $NADH/NAD^+$ couple is directly linked to GAPDH, and an increase in the $NADH/NAD^+$ ratio (caused by capturing of extracellular acetaldehyde with cyanide) effectively inhibits GAPDH, leading to higher F16P concentrations and thereby making PFK more sensitive for ATP inhibition.

The increase in the $NADH/NAD^+$ ratio caused by acetaldehyde efflux as stimulated by cyanide addition, and its inhibition of GAPDH, is a second mechanism (in addition to the *tps1*Δ phenotype) leading to accumulation of hexose phosphates. We could prevent the phenotype associated with this second mechanism, which is not caused by unregulated glucose transport and phosphorylation but is due to GAPDH inhibition, by increasing the capacity of the glycerol branch.

We validated a detailed glycolytic model for yeast glycolytic oscillations by testing its compliance with

available data from a diverse set of experiments. For most of the experiments, the model had a high predictive power, indicating that the existing knowledge on enzyme kinetics as collected in the model is sufficient to simulate a large set of experiments qualitatively and some even quantitatively. For two experiments, the model displayed qualitatively different behavior than observed in experiments: the frequency dependency for glucose and the cyanide bifurcation diagram. For both phenomena, it appeared that the lack of detail that is currently available for the description of the storage carbohydrate branches may be responsible, at least partly, for the discrepancies between model and experiment. Another branch to the glycolytic pathway that was not modeled in detail in the Teusink model was the glycerol branch, which is important to overcome *tps1*Δ-like behavior of the model.

Our results indicate that models constructed on the basis of experimentally measured parameter values can have a large predictive value, and may be reusable in other studies. This is an important result for the Silicon Cell initiative [Snoep J.L. (2005) The Silicon Cell initiative: working towards a detailed kinetic description at the cellular level. *Current Opinions in Biotechnology* **16**, 336–343.] and for systems biology efforts in general. Strikingly, the inadequacy of the model to simulate some experiments appears to be related to branches in the glycolytic pathway for which we currently have no accurate kinetic detail, stressing again the importance of accurate experimentally measured enzyme kinetics. It is unclear how generic these results are for other systems, but the high predictive value of a detailed kinetic model created for a different *S. cerevisiae* strain incubated under different conditions is encouraging.

Acknowledgements

We acknowledge financial assistance from the UK Biotechnology and Biological Sciences Research Council to F.dP. and J.L.S. via a SysMO-DB grant, and from the National Research Foundation in South Africa to D.D.vN. and J.L.S.

References

1 Oreskes N, Shrader-Frechette K & Belitz K (1994) Validation, and confirmationof numerical models in the earth sciences. *Science* **263**, 641–646.
2 Beck M, Ravetz J, Mulkey L & Barnwell T (1997) On the problem of model validation for predictive exposure assessments. *Stoch Hydrol Hydraul* **11**, 229–254.
3 Nyman E, Cedersund G & Stralfors P (2012) Insulin signaling – mathematical modeling comes of age. *Trends Endocrinol Metab* **23**, 107–115.
4 Teusink B, Passarge J, Reijenga CA, Esgalhado E, Van der Weijden CC, Schepper M, Walsh MC, Bakker BM, Van Dam K, Westerhoff HV *et al.* (2000) Can yeast glycolysis be understood in terms of *in vitro* kinetics of the constituent enzymes? Testing biochemistry. *Eur J Biochem* **267**, 5313–5329.
5 du Preez FB, van Niekerk DD, Kooi B, Rohwer JM & Snoep JL (2012) From steady-state to synchronized yeast glycolytic oscillations I: model construction. *FEBS J* **279**, doi: 10.1111/j.1742-4658.2012.08665.x.
6 Westerhoff HV & Palsson BO (2004) The evolution of molecular biology into systems biology. *Nat Biotechnol* **22**, 1249–1252.
7 Ashyraliyev M, Fomekong-Nanfack Y, Kaandorp JA & Blom JG (2009) Systems biology: parameter estimation for biochemical models. *FEBS J* **276**, 886–902.
8 Cedersund G & Roll J (2009) Systems biology: model based evaluation and comparison of potential explanations for given biological data. *FEBS J* **276**, 903–922.
9 Kreutz C & Timmer J (2009) Systems biology: experimental design. *FEBS J* **276**, 923–942.
10 Gustavsson A-K, van Niekerk DD, Adiels CB, du Preez F, Goksör M & Snoep JL (2012) Sustained glycolytic oscillations in individual isolated yeast cells. *FEBS J*, **279**, doi: 10.1111/j.1742-4658.2012.08639.x.
11 Richard P, Teusink B, Hemker MB, Dam KV & Westerhoff HV (1996) Sustained oscillations in free-energy state and hexose phosphates in yeast. *Yeast* **12**, 731–740.
12 Ghosh A, Chance B & Pye E (1971) Metabolic coupling and synchronization of NADH oscillations in yeast cell populations. *Arch Biochem Biophys* **145**, 319–331.
13 Richard P, Bakker BM, Teusink B, Dam KV & Westerhoff HV (1996) Acetaldehyde mediates the synchronization of sustained glycolytic oscillations in populations of yeast cells. *Eur J Biochem* **235**, 238–241.
14 Hynne F, Danø S & Sørensen P (2001) Full-scale model of glycolysis in *Saccharomyces cerevisiae*. *Biophys Chem* **94**, 121–163.
15 Danø S, Sørensen P & Hynne F (1999) Sustained oscillations in living cells. *Nature* **402**, 320–322.
16 Thevelein JM & Hohmann S (1995) Trehalose synthase: guard to the gate of glycolysis in yeast? *Trends Biochem Sci* **20**, 3–10.
17 Reijenga KA, van Megen YM, Kooi BW, Bakker BM, Snoep JL, van Verseveld HW & Westerhoff HV (2005) Yeast glycolytic oscillations that are not controlled by a single oscillophore: a new definition of oscillophore strength. *J Theor Biol* **232**, 385–398.
18 Reijenga KA, Snoep JL, Diderich JA, van Verseveld HW, Westerhoff HV & Teusink B (2001) Control of

glycolytic dynamics by hexose transport in *Saccharomyces cerevisiae*. *Biophys J* **80**, 626–634.
19 Rossell S, van der Weijden C, Lindenbergh A, van Tuijl A, Francke C, Bakker B & Westerhoff H (2006) Unraveling the complexity of flux regulation: a new method demonstrated for nutrient starvation in *Saccharomyces cerevisiae*. *Proc Natl Acad Sci USA* **103**, 2166–2171.
20 Albers E, Larsson C, Andlid T, Walsh MC & Gustafsson L (2007) Effect of nutrient starvation on the cellular composition and metabolic capacity of *Saccharomyces cerevisiae*. *Appl Environ Microbiol* **73**, 4839–4848.
21 Das J & Busse H (1991) Analysis of the dynamics of relaxation type oscillation in glycolysis of yeast extracts. *Biophys J* **60**, 369–379.
22 Nielsen K, Sørensen PG, Hynne F & Busse HG (1998) Sustained oscillations in glycolysis: an experimental and theoretical study of chaotic and complex periodic behavior and of quenching of simple oscillations. *Biophys Chem* **72**, 49–62.
23 Ozalp V, Pedersen T, Nielsen L & Olsen L (2010) Time-resolved measurements of intracellular ATP in the yeast *Saccharomyces cerevisiae* using a new type of nanobiosensor. *J Biol Chem* **285**, 37579–37588.
24 De Monte S, d'Ovidio F, Danø S & Sorensen PG (2007) Dynamical quorum sensing: population density encoded in cellular dynamics. *Proc Natl Acad Sci USA* **104**, 18377–18381.
25 Danø S, Madsen M & Sørensen P (2007) Quantitative characterization of cell synchronization in yeast. *Proc Natl Acad Sci USA* **104**, 12732–12736.
26 Blazquez MA, Lagunas R, Gancedo C & Gancedo JM (1993) Trehalose-6-phosphate, a new regulator of yeast glycolysis that inhibits hexokinases. *FEBS Lett* **329**, 51–54.
27 Galazzo J & Bailey J (1990) Fermentation pathway kinetics and metabolic flux control in suspended and immobilized *Saccharomyces cerevisiae*. *Enzyme Microbial Technol* **12**, 162–172.
28 Reijenga K, Westerhoff H, Kholodenko B & Snoep J (2002) Control analysis for autonomously oscillating biochemical networks. *Biophys J* **82**, 99–108.
29 Wolf J, Passarge J, Somsen OJ, Snoep JL, Heinrich R & Westerhoff HV (2000) Transduction of intracellular and intercellular dynamics in yeast glycolytic oscillations. *Biophys J* **78**, 1145–1153.